Received: 26 October 2023 | Revised: 13 March 2024 | Accepted: 7 April 2024

DOI: 10.1002/ctpp.202300139

ORIGINAL ARTICLE

Contributions to Plasma Physics

First SOLPS-ITER simulations of ASDEX Upgrade partially detached H-mode with boron impurity: The missing radiation at the outer strike-point region

S. O. Makarov[1] | D. P. Coster[1] | T. Gleiter[1] | D. Brida[1] | M. Muraca[1] | R. Dux[1] | P. David[1] | B. Kurzan[1] | X. Bonnin[2] | M. O'Mullane[3,4] | ASDEX Upgrade Team[*]

[1]Max-Planck-Institut für Plasmaphysik, Garching, Germany

[2]ITER Organization, St-Paul-Lez-Durance, France

[3]Culham Science Centre, UKAEA, Abingdon, UK

[4]Dept. Physics, University of Strathclyde, Glasgow, UK

Correspondence
S. O. Makarov, Max-Planck-Institut f¨ur Plasmaphysik, D-85748 Garching, Germany.
Email: sergei.makarov@ipp.mpg.de

Funding information
the EUROfusion Consortium; European Union via the Euratom Research and Training Programme, Grant/Award Number: 101052200

Abstract

Partially detached H-modes are the baseline regime for the future ITER operation. The ASDEX Upgrade partially detached H-mode is modeled using the SOLPS-ITER code with drifts enabled and compared with experimental data. For the first time, boron (B) impurity is simulated in the Scrape-off layer (SOL) and divertor. A comparison between divertor diagnostics and discrepancies between Langmuir probe and Divertor Thomson scattering/Stark broadening diagnostic are discussed. In the modeling, experimental target profiles are reproduced if the experimental level of radiation in the SOL and divertor is achieved using nitrogen (N) impurity seeding. Bolometry measurements detect substantial radiation from the partially detached outer strike point. With B radiation, this maximum in bolometry data is reproduced in the modeling, which is not possible with N alone.

KEYWORDS

ASDEX Upgrade, bolometry, boron, modeling, SOLPS

1 | INTRODUCTION

Boron (B) is used for the plasma-facing components (PFC) coating, which significantly improves the performance of plasma operation in magnetic fusion devices, optimising first wall recycling and minimising the impurity concentration in the plasma.[1] The boronization procedure is routinely performed in the full tungsten (W) wall tokamak ASDEX Upgrade (AUG). The old AUG boronization system[2] required evacuating the building due to the presence of the highly toxic diborane gas. The improved boronization system[3] allows more frequent and controlled boronization process without the need for personnel evacuation. The B wall conditioning extends the AUG operational space to the low gas puff scenarios avoiding core W accumulation.[1] In the current ITER design, the first wall consists of beryllium (Be). However, a change of the ITER first-wall material from Be to W is being considered. Moreover, many other fusion device designs (such as EU-DEMO,[4] CFETR,[5] and SPARC[6]) include a W first wall. The current boronization method is not applicable for long pulse reactor operations lasting 0.5–2 h. However, real-time B coating systems offer the potential for in-situ boronization

[*]See the author list in U. Stroth *et al* 2022 *Nucl. Fusion* **62** 042006.

during the discharge phase.[7] B layers on W surfaces produce B impurities, which lead to plasma dilution and impurity radiation. Thus, it is important to investigate the B contribution to the total radiation in present-day devices.

The ITER divertor must operate with target heat loads below $10 MW/m^2$.[8] SOLPS-ITER[9,10] modeling suggests[11,8] that partially detached conditions at the outer divertor target should be achieved to reliably control target heat loads within acceptable levels. Partially detached conditions are studied in present-day machines, such as AUG[12] and are modeled with the SOLPS-ITER code package for AUG and ITER.[13,14] This regime is studied with the SOLPS-ITER code and compared with the AUG experiment in this work where B impurity radiation in the partially detached divertor is analyzed.

2 | EXPERIMENTAL AND MODELING SETUP

In AUG, dedicated discharges with nitrogen (N) seeding were conducted[12] for obtaining 2D distributions of electron density (n_e) and temperature (T_e) in the divertor region using the Divertor Thomson scattering diagnostic (DTS). The partially detached ELMy H-mode discharge (#39,409), which is denoted as $T_{div} = 5 eV$ in reference [12], is analysed in this work. We note that in reference[13], the discharge #28,903 is simulated, which has different divertor target plate configurations, magnetic equilibrium, heating sources, outer midplane and outer target profiles. Thus, our simulations can not be directly related to the ones in reference [13].

Simulations are performed using the SOLPS-ITER code package[9,10] with drifts and currents enabled. Neutrals are treated kinetically by means of the "Monte-Carlo" EIRENE code.[15,16] Also, neutral-neutral collisions are taken into account in the simulations.

For the simulation, the magnetic equilibrium at 3.2 s in the discharge #39,410 is used, which is close to the magnetic equilibrium at 3.2 s in discharge #39,409 (Figure 2a represents the magnetic equilibrium vertical sweep for different time points). The flux-surface-averaged electron (Q_e) and ion heat (Q_i) fluxes at the pedestal entrance are imposed in the simulations as input parameters. First, the ASTRA code package[17,18] is used to calculate absorbed power by electrons and ions from Neutral Beam Injection (NBI) with the RABBIT module[19] and Electron Cyclotron Resonance Heating (ECRH) with the TORBEAM module.[20] Then, the radiated power inside the separatrix is estimated using the bolometry diagnostic (BLB) reconstruction.[21] As a result, $P_{sep} \sim 6 - 7 MW$ of power crossing the separatrix is observed in the experiment. Further analysis of the radiation in the scrape-off layer (SOL) and the power loads at the outer (OT) and inner targets (IT) suggests that P_{sep} is rather closer to $6 MW$.

Second, close to $Q_i/Q_e \approx 1.0$ is calculated at the pedestal top using our interpretive ASTRA simulations. However, the Q_i/Q_e is very sensitive to the relative positions of the T_e or T_i core profiles due to the strong temperature difference dependence in the electron-ion heat exchange ($S^{Ei\to e}_{e(i)} \propto T_e^{-3/2}(T_e - T_i)$[22]). In the simulations, a small sensitivity test is performed. The $Q_i/Q_e = 1.0$ (main simulation set up, which is used in this paper: $Q_i = 3.0 MW$ and $Q_e = 3.0 MW$) and $Q_i/Q_e = 2.6$ (test case simulation set up: $Q_i = 4.4 MW$ and $Q_e = 1.7 MW$) are tested to obtain the Q_i/Q_e contribution to the radiation in the divertor. Nonetheless, our main results regarding B radiation contribution, which we show for the $Q_i/Q_e = 1.0$ case in Section 5, are reproduced also for the $Q_i/Q_e = 2.6$ choice. The total radiation profile in the divertor region is not very sensitive to the Q_i/Q_e ratio at the core boundary. For both cases with $Q_i/Q_e = 1.0$ and $Q_i/Q_e = 2.6$, the total poloidal heat flux at the divertor entrance (X-point level) is predominantly channeled through the electron heat transport mechanism. This is due to the highly efficient process of electron-ion equilibration and the parallel electron heat conductance within the SOL.

The D puffing location is chosen in the private flux region (PFR) according to the experimental setup, which is a standard puffing location for the AUG experiment and simulations.[23] The puffing rate $\Gamma_D^{puff} = 2.0 \cdot 10^{22} D/s$ is taken according to the experimental measurements of the gas injection valves.[24] The core source is set $\Gamma_D^{core} = 8.0 \cdot 10^{20} D/s$ mimicking the source due to NBI. The sub-divertor neutral conductance structures, similar to thouse used in reference[25], are included in the simulations. In the simulation, the neutral pressure in the sub roof baffle volume is $p_0^{SOLPS} = 2.4 Pa$, which is close to the one measured directly by the pressure gauge $p_0^{gauge} = 2.7 Pa$ or to the one inferred from the High field side (HFS) baratron measurements $p_0^{baratron} = 2.6 Pa$.[26] Thus, the effective pumping speed, which is introduced via sub-divertor neutral conductance and cryo-pump albedo, is chosen correctly in the modeling. We note, matching sub-divertor neutral pressure and OT profiles at the same time is problematic without drifts activated.[23,27] For the test, we switched off drifts and obtained similar sub-divertor pressure because the effective pumping speed and throughputs were left unchanged. However, OT and IT profiles are changed completely and can not be matched with the experiment.

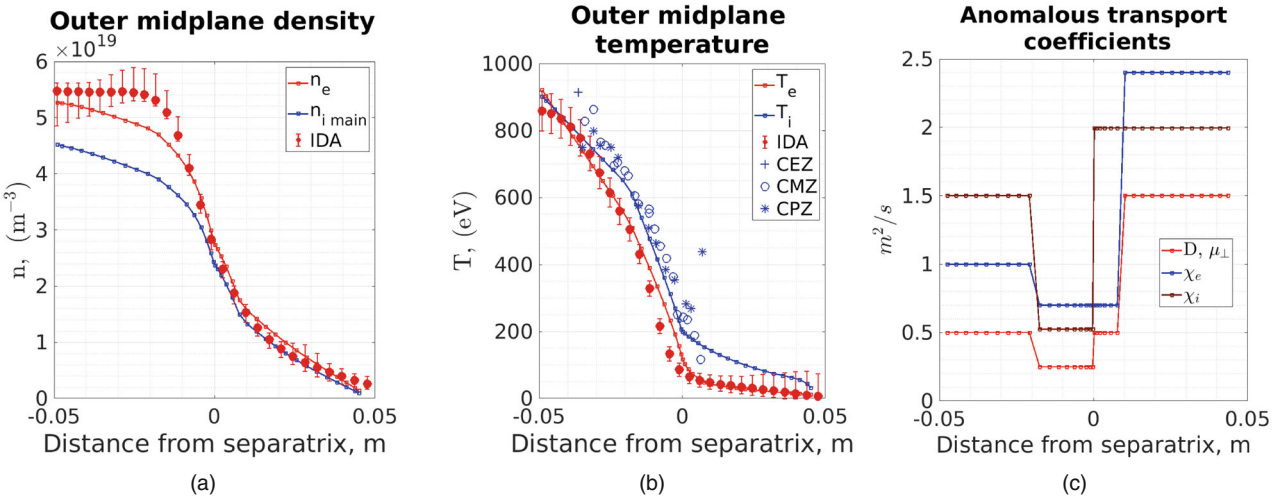

FIGURE 1 OMP profiles: (a) SOLPS-ITER n_e and main ion density ($n_{i\,main}$) (solid line). Experimental integrated data analysis (IDA) n_e (filled circles). (b) SOLPS-ITER T_e and T_i (solid line). Experimental IDA T_e (filled circles) and Charge exchange recombination spectroscopy (CXRS) T_i (pluses, hollow circles, asterisks). OMP anomalous transport coefficients: (c) diffusivity coefficient (D), viscosity coefficient ($\mu_\perp$), electron (χ_e) and ion (χ_i) heat conductivities.

The anomalous transport coefficients (Figure 1c) are chosen in order to reasonably match n_e, T_e and T_i OMP experimental profiles (Figure 1a,b) for the given D flux, Q_e and Q_i, respectively. Those are close to the ones routinely used for the AUG SOLPS-ITER simulations.[13]

Based on BLB measurements, the total radiation in the SOL (above $Z=-0.72$ m) was $S_e^{Rad\,SOL\,exp}=1.1MW$ and in the divertor region (below $Z=-0.72$ m) excluding radiation inside the separatrix was $S_e^{Rad\,div\,exp}=2.5MW$. N impurity is seeded (at the same place as D puffing) in the simulation in order to achieve similar radiation in the SOL and divertor. Namely, the N radiation (integrated over the SOL and divertor domains) $S_{e(N)}^{Rad\,SOLPS}=2.9MW$ and the deuterium (D) radiation (integrated over the SOL and divertor domains) $S_{e(D)}^{Rad\,SOLPS}=0.7MW$ are achieved. As a result, the partially detached OT, with integral OT power load $Q_{tot}^{OT}=1.7MW$, is obtained in the simulation.

3 | OUTER TARGET PROFILES: EXPERIMENTAL DATA

Before discussing SOLPS-ITER OT profiles, it is worthwhile to analyze the experimental diagnostics at the OT. In the experiment (shot #39,409, which is denoted as $T_{div}=5eV$ in reference [12]), the magnetic equilibrium is swept vertically as shown in Figure 2a. We note that independent of the magnetic equilibrium position, the flush-mounted triple Langmuir probe (LP) "ua6"[28] (magenta circle) and DTS "channel 2"[29] (black dash) measure plasma parameters near the target surface at similar poloidal positions (the distance along the target between LP "ua6" and DTS "channel 2" is 1 cm). Thus, following time traces of the LP "ua6" and DTS "channel 2" measurements, one can plot (see Figure 2b) the T_e profile along the target with respect to the distance from the separatrix/strike-point (the 1 cm difference between LP "ua6" and DTS "channel 2" is taken into account). It is worth mentioning that the DTS measurements are not affected by the magnetic sheath whereas LP measurements depend on the applied magnetic sheath model (more details are provided later in this section).

In the far-SOL (when distance from the separatrix $>4cm$), both the LP "ua6" and DTS "channel 2" show attached-like $T_e=13eV$. However, as depicted in Figure 2b, in the near-SOL (when distance from the separatrix $<4cm$), the DTS "channel 2" observes detached-like $T_e=1-2eV$, whereas LP "ua6" observes attached-like $T_e=15eV$. Furthermore, in the PFR the DTS T_e is much smaller than LP T_e (Figure 2b).

Similarly, one can consider OT n_e profiles. As shown in Figure 3a, the far-SOL ($>4cm$) DTS and LP n_e measurements match each other. We note, the LP n_e is measured at the sheath entrance, whereas the DTS n_e is measured in the plasma volume. Nonetheless, in the conduction-limited regime[30] (here in the specific flux tube) the temperature decrease can be comparable to the static pressure decrease. In this case the n_e variation along the flux tube is smaller than in the two

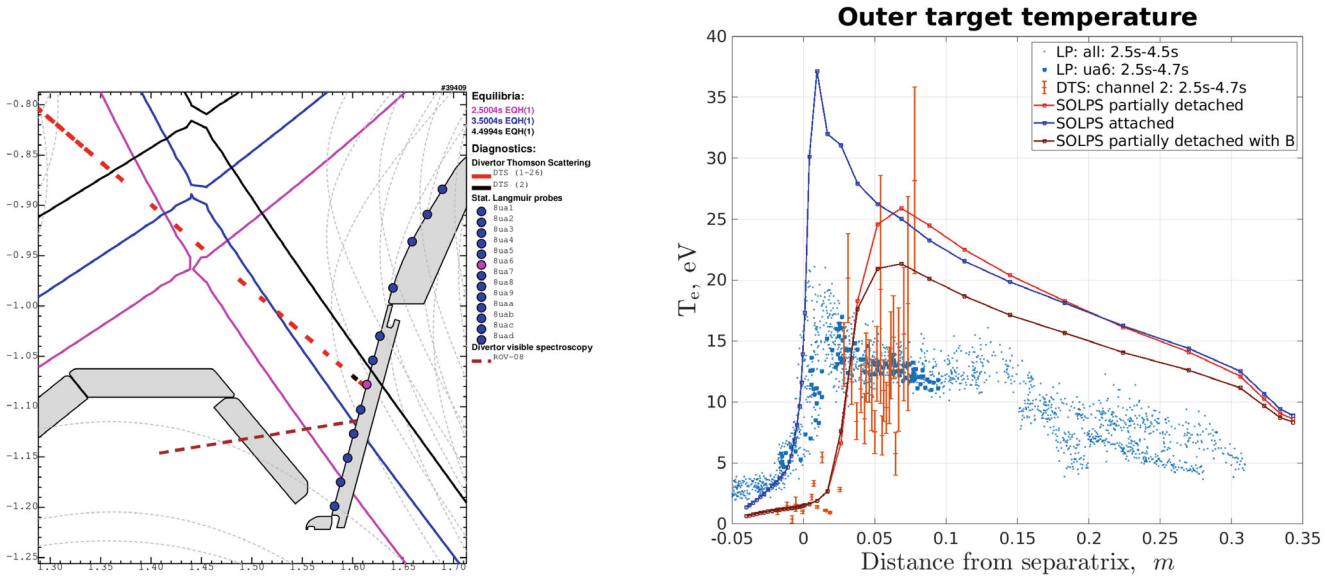

FIGURE 2 (a) Divertor diagnostic set: LP all (blue circles) and LP "ua6" (magenta circle). DTS (red dashes) and DTS "channel 2" (black dash). SBD (EVL spectrometer) "ROV-08" LOS (brown dashed line). For the magnetic equilibrium vertical sweep, the LP and DTS time traces are plotted along the target with respect to the separatrix: (b) OT T_e target profile. Experimental: LP all (blue dots) and LP "ua6" (blue squares). DTS "channel 2" (red pluses). SOLPS-ITER: with N seeding rate $3.0 \cdot 10^{20}\, atoms/s$ (red solid line), with N seeding rate $0.8 \cdot 10^{20}\, atoms/s$ (blue solid line) and with N seeding rate $3.0 \cdot 10^{20}\, atoms/s$ and B (brown solid line).

times decrease from the upstream towards the sheath entrance in the isothermal sheath limited case.[31] For instance, this non-isothermal scenario is found in the SOLPS-ITER simulations (Section 4): in the flux tube, which is chosen $5\,cm$ from the separatrix Figure 3a, the n_e variation along the flux tube is $< 20\%$. Therefore, it is expected that the LP sheath entrance density and the DTS volumetric density are close to each other.

In the near-SOL ($< 4\,cm$), DTS "channel 2" shows substantial increase of the $n_e = 2 - 4 \cdot 10^{20}\, m^{-3}$. There are independent measurements of n_e available by the Stark broadening diagnostic (SBD).[32] The (SBD) measurements are non-local, that is, the measured n_e comes from the spatial maximum of the Balmer-ϵ and Balmer-δ emissions. However, analyzing 2D DTS n_e profiles (Figure 9e in reference [12]) it can be shown that around 3.7 s the line of sight (LOS) ROV-08 (Figure 2a) measures n_e maximum from the strike-point region and the contribution from n_e in the PFR part of the LOS ROV-08 is negligible. Thus, similar to the DTS, the SBD provides large $n_e = 4 \cdot 10^{20}\, m^{-3}$ at the near-SOL region in the vicinity of the target surface (Figure 3a). However, LP shows $n_e < 1 \cdot 10^{20}\, m^{-3}$ in the near-SOL contrary to DTS and SBD results. Note, the LP n_e is calculated from the LP T_e and the LP ion saturation current (j_{sat}) using $n_e = j_{sat} / \left(e\sqrt{2T_e e/(m_i)} sin(\alpha) \right)$ (here, α is an angle between magnetic field and target surface). Thus, the low value of the LP n_e is an independent indication of the LP T_e overestimation.

As depicted in Figure 3b, the j_{sat}, which is estimated from the DTS n_e and the DTS T_e using $j_{sat} = en_e\sqrt{2T_e e/(m_i)}$ $sin(\alpha)$, is found close to the measured LP j_{sat}. There is no independent measurement for the SBD T_e. One can estimate j_{sat} using the SBD n_e and detached-like $T_e = 1\,eV$ (Figure 3b) and obtain similar values to the LP j_{sat} and the DTS j_{sat} (for $T_e = 15\,eV$ SBD j_{sat} would be notably larger). Based on this diagnostics cross-check we confirm reliable LP j_{sat} measurements for this discharge. It is expected that the LP j_{sat} observations are more solid than the LP T_e ones, which are strongly dependent on the exact sheath model which is used for the triple probe a 4-parameter fitting Equation (2) in reference [33], which is not reliable for the regimes that are close to detachment. One should be careful with triple LP T_e measurements in such regimes. It is worth to note that even in attached L-mode regimes, discrepancies between DTS and LP T_e measurements were reported in DIII-D.[34] One of the possible reasons for the large LP T_e could be an electron non-Maxwellian tail, which can greatly modify a current–voltage characteristic of LP,[35] which violates our 4-parameter fitting expression assumption. Summarising this diagnostic cross-comparison exercise, we conclude that for the discharge #39,409, the T_e is greatly overestimated by the LP, and the OT T_e profile is represented correctly by the DTS (Figure 2b).

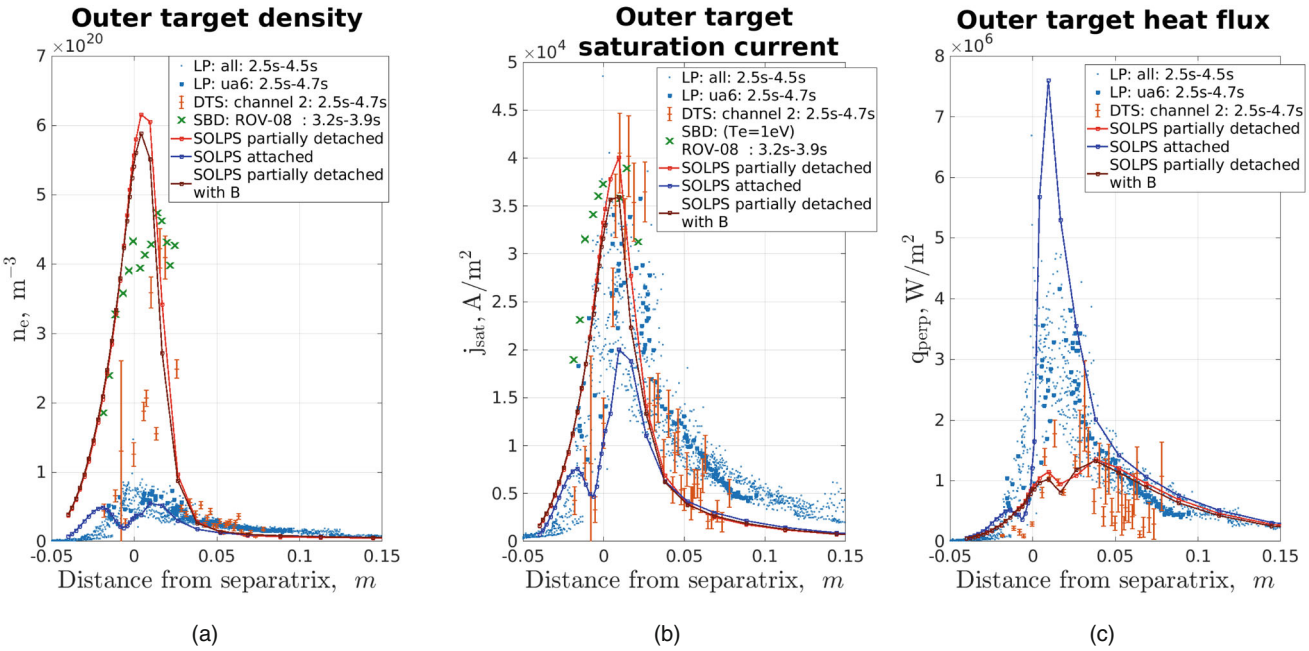

FIGURE 3 Experimental: LP all (blue dots) and LP "ua6" (blue squares). DTS "channel 2" (red pluses). SBD "ROV-08" (green crosses). SOLPS-ITER: with N seeding rate $3.0 \cdot 10^{20}\, atoms/s$ (red solid line), with N seeding rate $0.8 \cdot 10^{20}\, atoms/s$ (blue solid line) and with N seeding rate $3.0 \cdot 10^{20}\, atoms/s$ and B (brown solid line). OT profiles: (a) n_e, (b) j_{sat}, (c) q_{perp}.

In the near-SOL, T_e contributes significantly to the heat flux impinging onto the target surface. Attached-like T_e leads to the attached-like LP target heat flux $q_{perp} = 4 - 5 MW/m^2$ (Figure 3c), which is estimated by the simplified

$$q_{perp} = j_{sat} \cdot (T_e \cdot (5 + 2) + 13.6 + 5.5/2) \tag{1}$$

expression[36] from the LP T_e and j_{sat} data. Similarly, one can get q_{perp} values based on DTS measurements. Thus, as shown in Figure 3c the partially detached DTS $q_{perp} = 1 - 2 MW/m^2$ heat flux is obtained. The difference between attached and partially detached values of the heat flux is crucial for the investigation of the partially detached regimes, which are expected to be achieved in ITER.[11,8]

4 | SOLPS-ITER MODELING RESULTS

As discussed in Section 2, with $S_{e(N)}^{Rad\,SOLPS} = 2.9\,MW$, the partially detached conditions are achieved by seeding N at the rate $\Gamma_N = 3.0 \cdot 10^{20}\, atoms/s$. In Figures 2b and 3a–c, red curves represent target profiles for these partially detached conditions. Additionally, the attached regime with lower N seeding rate $\Gamma_N = 0.8 \cdot 10^{20}\, atoms/s$ is shown by the blue curve for comparison. Contrary to the attached conditions, in the partially detached regime the high n_e and low T_e zone forms in the vicinity of the strike point resulting in the smaller q_{perp} (see Figure 3c). It is worthwhile to note that at $0.00 - 0.01\, m$ distances from separatrix, ($T_e \approx 1\, eV$) the dominant part of the $q_{perp} \approx 1 MW/m^2$ is recombination due to large j_{sat}, which is represented by the last two terms in the simplified expression (1). However, at $0.04 - 0.05\, m$ distances from separatrix ($T_e \approx 20\, eV$), the heat flux contribution of the $q_{perp} \approx 1 MW/m^2$, which is represented by the first two terms in Equation (1), is the largest. In the partially detached regime the radiation fraction in q_{perp} becomes substantial (up to 50% at specific locations), which is taken into account in the simulation, but not captured in Equation (1).

We note that the partially detached j_{sat} is even larger than the attached one (see Figure 3b). This represents a fundamental difference between the partially and fully detached regimes, in which j_{sat} is smaller than the attached j_{sat} (j_{sat} rollover).

In Figure 4a,b, the 2D n_e and T_e SOLPS-ITER distributions are plotted. Those reproduce fairly closely the ones that were reconstructed from DTS in Figures 9d and 9e in reference [12] Particularly, high n_e on the HFS and in the PFR.

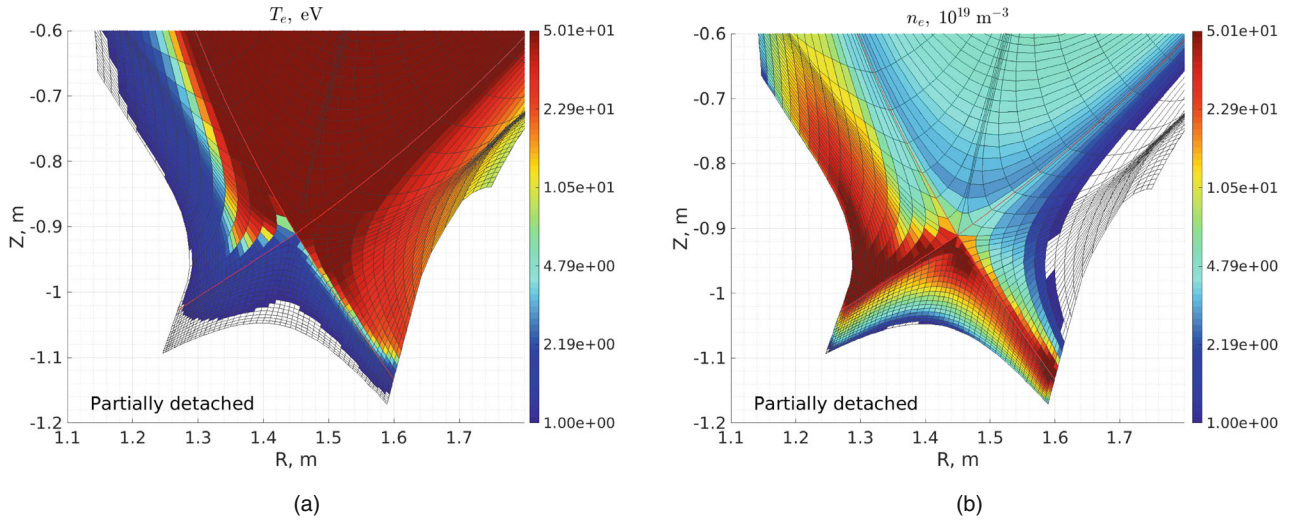

FIGURE 4 Partially detached SOLPS-ITER 2D distributions in the divertor: (a) T_e, (b) n_e (colour bar is in the log scale). The maximum and minimum of the color scales are similar to corresponding in Figure 9d,e in reference [12].

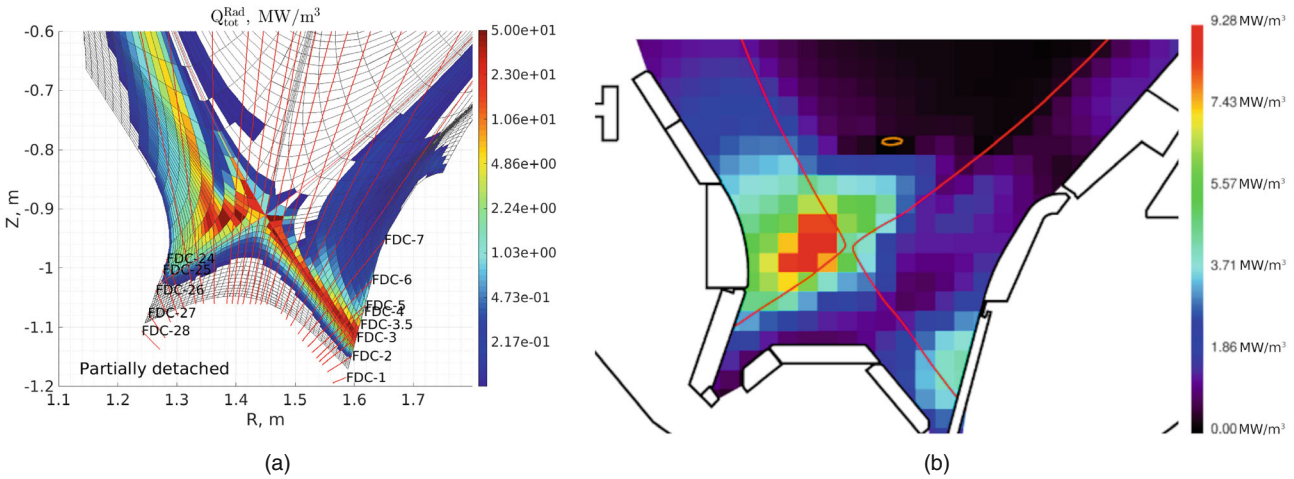

FIGURE 5 (a) SOLPS-ITER 2D distribution of total radiation (colour bar is in the log scale). Red lines represent BLB LOSs. The "FDC-3.5" LOS is artificially added into the SOLPS-ITER synthetic diagnostic to fill the gap between "FDC-3" and "FDC-4". (b) 2D bolometry tomographic reconstruction.

Also, the high n_e and low T_e area in the vicinity of the strike point is well reproduced in the 2D n_e and T_e SOLPS-ITER distributions (Figure 4a,b). This zone can be also observed in the 2D DTS reconstructions (Figure 9d,e in reference [12]).

Experimental divertor target profiles are reasonably well reproduced by the partially detached SOLPS-ITER simulations (red in Figures 2b and 3a–c). However, we note larger near-SOL n_e, larger far-SOL T_e and smaller far-SOL j_{sat} in the simulation. The reason for these discrepancies is under investigation.

Furthermore, it is worthwhile to study the radiation in the divertor. The HFS radiation maximum, which is observed in the 2D BLB reconstruction (Figure 5b), is reproduced in the modeling (Figure 5a). However, the radiation peak near the outer strike point, which can be seen in Figure 5b, does not appear in the simulations. This discrepancy can be observed even more clearly, if the radiation integrated along the specific LOSs (Figure 5a) is compared with the BLB measurements. In Figure 6a, the BLB diagnostic clearly detects radiation peaking at the FDC-3 channel, which is pointing at the outer strike point. D radiation (yellow in Figure 6a) is too small to explain this maximum. N radiation (purple in Figure 6a) is decreasing, while moving towards the FDC-3 channel. From the simplified local ionization equilibrium radiation model,[37] one can confirm that N does not radiate efficiently in the $T_e = 1 - 2eV$ zone in the vicinity of the outer

strike point. Adding more N leads only to the radiation front movement further from the target. However, B can radiate efficiently at such low temperatures.

5 | BORON RADIATION

The charge exchange recombination spectroscopy (CXRS) diagnostic[38] measures a non-negligible amount of B^{+5} in the discharge #39,409 in the core region $n_B^{core} = 1.2 \cdot 10^{17}\, ions/m^3$ (17 days between B coating, which was carried out on May 25, 2021, and discharge #39,409, which was carried out on June 11, 2021). This is comparable to the core N^{+7} CXRS measurements $n_N^{core} = 2.0 \cdot 10^{17}\, ions/m^{-3}$. These measurements are conducted during the 2.0–5.0 s phase of the discharge (chosen for simulation; the equilibrium vertical sweep is illustrated in Figure 2a) with a constant N seeding rate $8.1 \cdot 10^{20}\, atoms/s$. Thus, a comparable amount of B impurity is added into the simulation, to study B radiation contribution in the divertor region. In contrast to N, which is recycled on every surface except cryo-pumps, B is assumed to be absorbed by the surface, if it is not reflected according to the TRIM database.[15,39] Also, N is puffed in the PFR, whereas B is sputtered from the first wall and targets. An advanced wall dynamic model[40] and edge localised modes (ELMs) contribution should be taken into account to accurately calculate the B source. In our initial test simulations, we employed a highly constrained and simplified sputtering model. The primary objective of the modeling was to investigate any potential influence of B radiation on divertor behavior under conditions reflecting realistic B amounts. In our case, we use a free parameter "A" as a multiplier for the B surface Roth-Bogdanski sputtering yield[41] at every material surface (same for each surface in this test), to control the amount of B impurity in the simulation. The "A" parameter is set in order to achieve the n_B^{core}/n_N^{core} approaching unity in the modeling. The $n_B^{core}/n_N^{core} \approx 0.9$ is achieved in the simulation when A reached 1. Although this exceeds the experimental $n_B^{core}/n_N^{core} \approx 0.6$, it is deemed acceptable within the context of our testing framework.

In the simulation, the largest sputtering is obtained at the OT: $1.3 \cdot 10^{21}\, B/s$, whereas sputtering at the wall and at the IT are: $2.7 \cdot 10^{20}\, B/s$ and $5.5 \cdot 10^{16}\, B/s$, respectively. B accumulation at the outer strike point region is observed resulting in substantial B radiation in this area (Figure 7b). In Figure 7a, it can be observed that N radiation is located further from the target surface. Thus, by introducing additional B radiation (green curve in Figure 6b) it is possible to reproduce the experimental radiation maximum at the outer strike point (blue curve in Figure 6b). A remarkable peaking of the radiation profile is noted between channels 3 and 4 in the SOLPS-ITER modeling as illustrated by the orange curve in Figure 6b. Nonetheless, the observed experimental peak is 15% smaller than the corresponding peak in the SOLPS-ITER simulations. This discrepancy can be attributed predominantly to the arbitrary selection of the B source and inherent limitations in the sputtering model within our SOLPS-ITER simulations. We note that with N impurity alone, as N radiation decreases towards cold strike-point zone, and D radiation remains at a moderate level, as depicted in Figure 6a,b. Thus, B is a good

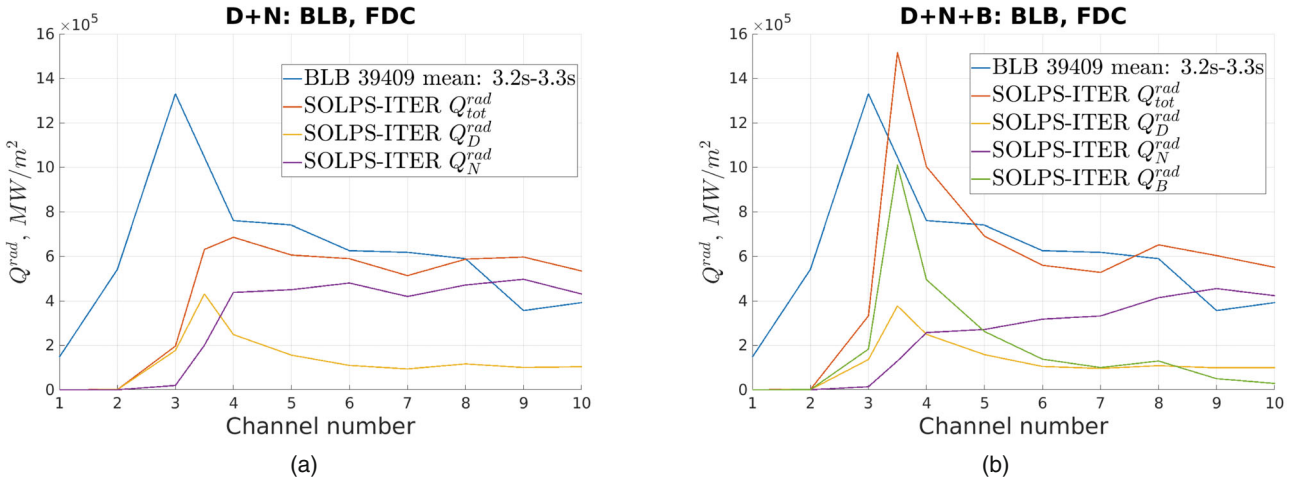

FIGURE 6 Line integrated radiation along BLB LOSs from FDC-1 to FDC-10 (see Figure 5a). Experimental measurements by BLB (blue). SOLPS-ITER modeling: total radiation (red), D radiation (yellow), N radiation (purple), B radiation (green). (a) D + N mixture. (b) D + N + B mixture.

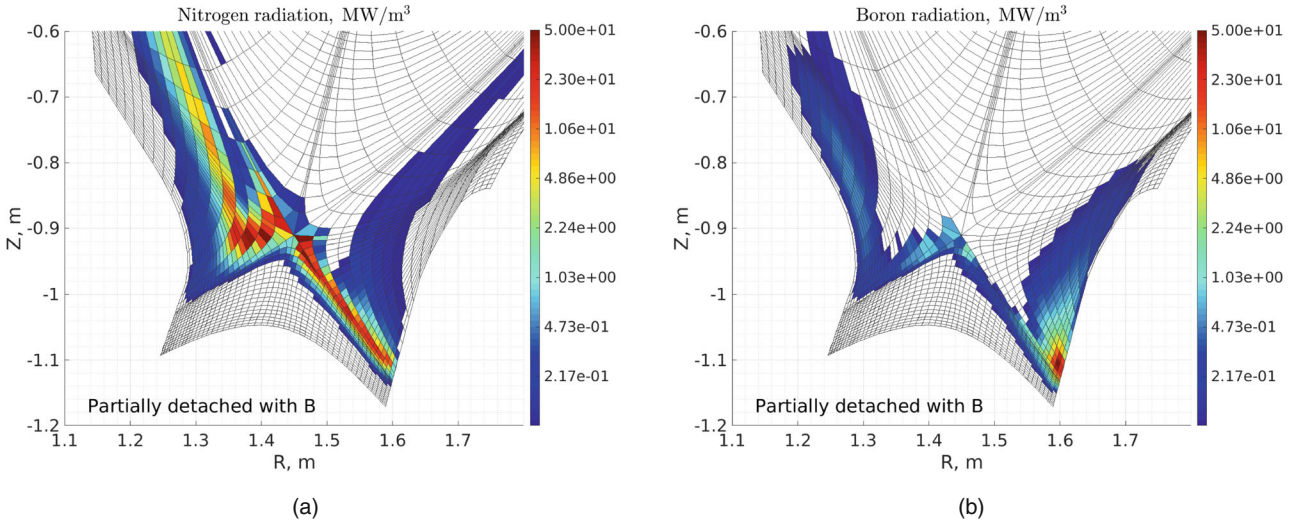

FIGURE 7 D + N + B SOLPS-ITER 2D distribution of impurity radiation (colour bar is in the log scale). (a) N radiation. (b) B radiation.

candidate to explain the missing radiation from the high n_e, low T_e region in the vicinity of the outer strike point in the partially detached AUG divertor.

We would like to emphasise that the experimental radiation profile is notably shifted towards the PFR in comparison to the SOLPS-ITER profile, as illustrated in Figure 6b. Significant radiation is experimentally observed along FDC-2 and FDC-1 channels. In contrast, SOLPS-ITER does not predict any radiation on the corner (FDC-2) or outside of (FDC-1) the simulation domain (Figure 5a). This discrepancy highlights the clear presence of plasma beyond the last simulated flux tube in the structured grid SOLPS-ITER version (3.0.8), limited by the roof baffle of the AUG (it can be seen, for instance, in Figure 2 in reference [42]). This exhibits a specific importance of the unstructured grid SOLPS-ITER version (3.2.0)[43,44] application for detailed divertor simulations.

However, the B radiation contributes relatively little to the total radiation in the divertor region, that is, $S_{e(B)}^{Rad\,SOLPS} = 0.5 MW$. Moreover, a decrease of N radiation in the outer divertor is observed for the D + N → D + N + B transition (Figure 6a,b). This change of N radiation requires complex impurity transport analysis, which is not performed for this test simulation. Thus, as depicted in Figures 2b and 3a–c, no large difference in the OT profiles is found, when the B impurity is included in the simulation. The decrease of the T_e in the far-SOL is related to the far-SOL B radiation (Figure 7b).

It is important to note that a new boron ADAS95 database, which is a provisional one, where the more advanced collisional-radiative model is applied,[45] is used in the simulations, because the simplified ADAS89 database, which is based on coronal model, is not sufficient for reliable impurity transport simulations. The new B dataset is of the same quality as the other light element generalised collisional-radiative (GCR) data. The radiation model is improved due to being based on R-matrix excitation data, rather than the extremely simple set of effective lines of the 89 data. Likewise, the ionization balance coefficients are full GCR rates rather than simple semi-empirical evaluations. Similarly to N and Ne,[46] large differences in the ionisation distributions are observed for ADAS95 versus ADAS89 tests (for details, see https://git.iter.org/projects/IMEX/repos/amns-adas/pull-requests/16/overview). We anticipate incorporating the boron ADAS96 database into our future simulations once it is officially released.

6 | CONCLUSIONS

For the first time, SOLPS-ITER simulations with B impurity were carried out. Partially detached H-mode in AUG was modeled and compared with experimental data. Cross-comparison between LP, DTS, and SBD divertor diagnostics showed that for the partially detached discharge #39,409, LP substantially overestimates T_e, whereas j_{sat} is measured correctly. DTS and SBD detect the high n_e, low T_e region in the vicinity of the outer strike point, which appears in the partially detached regime. SOLPS-ITER target profiles match the experimental ones reasonably well if the radiated power in the SOL and divertor matches the experimental BLB level. The HFS radiation maximum is captured in the simulations. B radiation in the high n_e, low T_e outer strike point helps to reproduce the local radiation maximum, which is seen in the

experiment by bolometry. This cannot be achieved with N alone. Nevertheless, the experimental radiation profile exhibits a shift toward the PFR in comparison to the SOLPS-ITER one. This discrepancy is likely associated with the limitations inherent in the structured grid version of the SOLPS-ITER code. Thus, B is a good candidate to explain the high radiation at the outer strike point in the partially detached conditions.

ACKNOWLEDGMENTS

This work has been carried out within the framework of the EUROfusion Consortium, funded by the European Union via the Euratom Research and Training Programme (Grant Agreement No 101052200—EUROfusion) This work was performed in part under the auspices of the ITER Scientist Fellow Network. The views and opinions expressed herein do not necessarily reflect those of the European Commission or of the ITER Organization.

DATA AVAILABILITY STATEMENT

The data that support the findings of this study are available from the corresponding author upon reasonable request.

REFERENCES

[1] A. Kallenbach, R. Dux, M. Mayer, R. Neu, T. Pütterich, V. Bobkov, J. C. Fuchs, T. Eich, L. Giannone, O. Gruber, A. Herrmann, L. D. Horton, C. F. Maggi, H. Meister, H. W. Müller, V. Rohde, A. Sips, A. Stäbler, J. Stober, *Nucl. Fusion* **2009**, *49*, 045007.
[2] V. Rohde, R. Dux, A. Kallenbach, K. Krieger, R. Neu, *J. Nucl. Mater.* **2007**, *363-365*, 1369.
[3] M. Dibon, V. Rohde, F. Stelzer, K. Hegele, M. Uhlmann, *Fusion Eng. Des.* **2021**, *165*, 112233.
[4] R. Neu, J. Riesch, J. W. Coenen, J. Brinkmann, A. Calvo, S. Elgeti, C. García-Rosales, H. Greuner, T. Hoeschen, G. Holzner, F. Klein, F. Koch, C. Linsmeier, A. Litnovsky, T. Wegener, S. Wurster, J. H. You, *Fusion Eng. Des.* **2016**, *109–111*, 1046.
[5] Y. T. Song, S. T. Wu, J. G. Li, B. N. Wan, Y. X. Wan, P. Fu, M. Y. Ye, J. X. Zheng, K. Lu, X. Gao, S. M. Liu, X. F. Liu, M. Z. Lei, X. B. Peng, Y. Chen, *IEEE Trans. Plasma Sci.* **2014**, *42*, 503.
[6] P. Rodriguez-Fernandez, A. J. Creely, M. J. Greenwald, D. Brunner, S. B. Ballinger, C. P. Chrobak, D. T. Garnier, R. Granetz, Z. S. Hartwig, N. T. Howard, J. W. Hughes, J. H. Irby, V. A. Izzo, A. Q. Kuang, Y. Lin, E. S. Marmar, R. T. Mumgaard, C. Rea, M. L. Reinke, V. Riccardo, J. E. Rice, S. D. Scott, B. N. Sorbom, J. A. Stillerman, R. Sweeney, R. A. Tinguely, D. G. Whyte, J. C. Wright, D. V. Yuryev, *Nucl. Fusion* **2022**, *62*, 042003.
[7] A. Bortolon, V. Rohde, R. Maingi, E. Wolfrum, R. Dux, A. Herrmann, R. Lunsford, R. M. McDermott, A. Nagy, A. Kallenbach, D. K. Mansfield, R. Nazikian, R. Neu, *Nucl Mater Energy* **2019**, *19*, 384.
[8] R. A. Pitts, X. Bonnin, F. Escourbiac, H. Frerichs, J. P. Gunn, T. Hirai, A. S. Kukushkin, E. Kaveeva, M. A. Miller, D. Moulton, V. Rozhansky, I. Senichenkov, E. Sytova, O. Schmitz, P. C. Stangeby, G. de Temmerman, I. Veselova, S. Wiesen, *Nucl Mater Energy* **2019**, *20*, 100696.
[9] S. Wiesen, D. Reiter, V. Kotov, M. Baelmans, W. Dekeyser, A. Kukushkin, S. Lisgo, R. Pitts, V. Rozhansky, G. Saibene, I. Veselova, S. Voskoboynikov, *J. Nucl. Mater.* **2015**, *463*, 480.
[10] X. Bonnin, W. Dekeyser, R. Pitts, D. Coster, S. Voskoboynikov, S. Wiesen, *Plasma Fusion Res.* **2016**, *11*, 1403102.
[11] E. Kaveeva, V. Rozhansky, I. Senichenkov, E. Sytova, I. Veselova, S. Voskoboynikov, X. Bonnin, R. Pitts, A. Kukushkin, S. Wiesen, D. Coster, *Nucl. Fusion* **2020**, *60*, 046019.
[12] M. Cavedon, B. Kurzan, M. Bernert, D. Brida, R. Dux, M. Griener, S. Henderson, E. Huett, T. Nishizawa, T. Lunt, O. Pan, U. Stroth, M. Wischmeier, E. Wolfrum, the ASDEX Upgrade Team, *Nucl. Fusion* **2022**, *62*, 066027.
[13] I. Senichenkov, A. Poletaeva, E. Kaveeva, I. Veselova, V. Rozhansky, D. Coster, X. Bonnin, R. Pitts, *Nucl Mater Energy* **2023**, *34*, 101361.
[14] V. Rozhansky, E. Kaveeva, I. Senichenkov, I. Veselova, S. Voskoboynikov, R. Pitts, D. Coster, C. Giroud, S. Wiesen, *Nucl. Fusion* **2021**, *61*, 126073.
[15] D. Reiter, M. Baelmans, P. Börner, *Fusion Sci. Technol.* **2005**, *47*, 172.
[16] D. V. Borodin, F. Schluck, S. Wiesen, D. Harting, P. Börner, S. Brezinsek, W. Dekeyser, S. Carli, M. Blommaert, W. Van Uytven, M. Baelmans, B. Mortier, G. Samaey, Y. Marandet, P. Genesio, H. Bufferand, E. Westerhof, J. Gonzalez, M. Groth, A. Holm, N. Horsten, H. J. Leggate, *Nucl. Fusion* **2022**, *62*(8), 086051.
[17] G. V. Pereverzev, P. N. Yushmanov, Report No. (IPP 5/98). **2002**.
[18] E. Fable, C. Angioni, F. J. Casson, D. Told, A. A. Ivanov, F. Jenko, R. M. McDermott, S. Y. Medvedev, G. V. Pereverzev, F. Ryter, W. Treutterer, E. Viezzer, the ASDEX Upgrade Team, *Plasma Phys. Controlled Fusion* **2013**, *55*, 124028.
[19] M. Weiland, R. Bilato, R. Dux, B. Geiger, A. Lebschy, F. Felici, R. Fischer, D. Rittich, M. van Zeeland, the ASDEX Upgrade Team, and the Eurofusion MST1 Team, *Nucl. Fusion* **2018**, *58*, 082032.
[20] E. Poli, A. Peeters, G. Pereverzev, *Comput. Phys. Commun.* **2001**, *136*, 90.
[21] P. David, M. Bernert, T. Pütterich, C. Fuchs, S. Glöggler, T. Eich, the ASDEX Upgrade Team, *Nucl. Fusion* **2021**, *61*, 066025.
[22] S. Braginskii, Reviews of Plasma Physics, edited by MA Leontovich Consultants Bureau, Vol. *1*, Consultants Bureau, New York **1965**.
[23] F. Reimold, M. Wischmeier, S. Potzel, L. Guimarais, D. Reiter, M. Bernert, M. Dunne, T. Lunt, *Nucl Mater Energy* **2017**, *12*, 193.
[24] T. Härtl, V. Rohde, V. Mertens, *Fusion Eng. Des.* **2015**, *96-97*, 265.
[25] F. Hitzler, Radiative Cooling of the Divertor Plasma with Argon and Nitrogen Seeding in the ASDEX Upgrade Tokamak, PhD thesis, Technischen Universität München, Munich, Germany **2020**.

[26] A. Kallenbach, H. J. Sun, T. Eich, D. Carralero, J. Hobirk, A. Scarabosio, M. Siccinio, the ASDEX Upgrade Team, and the Eurofusion MST1 Team, *Plasma Phys. Controlled Fusion* **2018**, *60*, 045006.
[27] F. Hitzler, M. Wischmeier, F. Reimold, D. P. Coster, the ASDEX Upgrade Team, *Plasma Phys. Controlled Fusion* **2020**, *62*, 085013.
[28] D. Brida, T. Lunt, M. Wischmeier, M. Bernert, D. Carralero, M. Faitsch, Y. Feng, T. Sehmer, B. Sieglin, W. Suttrop, E. Wolfrum, *Nucl. Fusion* **2017**, *57*, 116006.
[29] B. Kurzan, A. Lohs, G. Sellmair, M. Sochor, the ASDEX Upgrade Team, *J. Instrum.* **2021**, *16*, C09012.
[30] J. Wesson, D. Campbell, Tokamaks, Oxford engineering science series, Clarendon Press, New York **1997**.
[31] P. C. Stangeby, The plasma boundary of magnetic fusion devices, Vol. *224*, Institute of Physics Pub, Philadelphia, Pennsylvania **2000**.
[32] S. Potzel, M. Wischmeier, M. Bernert, R. Dux, H. Müller, A. Scarabosio, the ASDEX Upgrade Team, *Nucl. Fusion* **2013**, *54*, 013001.
[33] H. De Oliveira, P. Marmillod, C. Theiler, R. Chavan, O. Février, B. Labit, P. Lavanchy, B. Marlétaz, R. A. Pitts, the TCV team, *Rev. Sci. Instrum.* **2019**, *90*, 083502.
[34] P. C. Stangeby, J. D. Elder, J. A. Boedo, B. Bray, N. H. Brooks, M. E. Fenstermacher, M. Groth, R. C. Isler, L. L. Lao, S. Lisgo, G. D. Porter, D. Reiter, D. L. Rudakov, J. G. Watkins, W. P. West, D. G. Whytem, *J. Nucl. Mater.* **2003**, *883*, 313.
[35] P. C. Stangeby, *Plasma Phys. Controlled Fusion* **1995**, *37*, 1031.
[36] D. Carralero, S. Artene, M. Bernert, G. Birkenmeier, M. Faitsch, P. Manz, P. de Marne, U. Stroth, M. Wischmeier, E. Wolfrum, the ASDEX Upgrade Team, and the Eurofusion MST1 Team, *Nucl. Fusion* **2018**, *58*, 096015.
[37] T. Pütterich, E. Fable, R. Dux, M. O'Mullane, R. Neu, M. Siccinio, *Nucl. Fusion* **2019**, *59*, 056013.
[38] E. Viezzer, T. Pütterich, R. Dux, R. M. McDermott, the ASDEX Upgrade Team, *Rev. Sci. Instrum.* **2012**, *83*, 103501.
[39] D. Reiter, The EIRENE Code User Manual, Institut für Energie- und Klimaforschung – Plasmaphysik Forschungszentrum Jülich GmbH; P.O.B. 1913; D-52425 Jülich, Germany.
[40] K. Schmid, K. Krieger, S. Lisgo, G. Meisl, S. Brezinsek, J. Contributors, *Nucl. Fusion* **2015**, *55*, 053015.
[41] W. Eckstein, C. Garcia-Rosales, J. Roth, W. Ottenberger, Sputtering Data, Max-Planck-Institut für Plasmaphysik, Garching **1993**.
[42] I. Y. Senichenkov, E. G. Kaveeva, E. A. Sytova, V. A. Rozhansky, S. P. Voskoboynikov, I. Y. Veselova, D. P. Coster, X. Bonnin, F. Reimold, *Plasma Phys. Controlled Fusion* **2019**, *61*, 045013.
[43] I. Senichenkov, E. Kaveeva, V. Rozhansky, N. Shtyrkhunov, K. Dolgova, R. Ding, H. Si, G. Xu, *Contrib. Plasma Physics* **2024**, e202300136.
[44] W. Dekeyser, P. Boerner, S. Voskoboynikov, V. Rozhanksy, I. Senichenkov, L. Kaveeva, I. Veselova, E. Vekshina, X. Bonnin, R. Pitts, M. Baelmans, *Nucl. Mater. Energy* **2021**, *27*, 100999.
[45] Private communitcation.
[46] I. Senichnkov, E. Kaveeva, A. Poletaeva, A. Nichik, V. Rozhansky, I. Veselova, 29th IAEA Fusion Energy Conference (FEC 2023), Contributions, and Conference Material. **2023**.

How to cite this article: S. O. Makarov, D. P. Coster, T. Gleiter, D. Brida, M. Muraca, R. Dux, P. David, B. Kurzan, X. Bonnin, M. O'Mullane, ASDEX Upgrade Team , *Contrib. Plasma Phys.* **2024**, e202300139. https://doi.org/10.1002/ctpp.202300139